Nonlocal electron kinetics and excited state densities in a magnetron discharge in argon

I. A. Porokhova,[1,2] Yu. B. Golubovskii,[2] C. Csambal,[1] V. Helbig,[3] C. Wilke,[1] and J. F. Behnke[1]

[1]*Institute for Physics, Ernst-Moritz-Arndt University, Domstrasse 10a, D-17489 Greifswald, Germany*
[2]*St. Petersburg State University, Ulianovskaia 1, 195904 St. Petersburg, Russia*
[3]*Institute of Experimental Physics, Christian-Albrechts University, Kiel, Germany*

The densities of argon metastable $^3P_2$, and resonance $^1P_1$, $^3P_1$ states were measured along a cylindrical magnetron discharge radius by absorption spectroscopy using a narrow bandwidth single mode diode laser. The theoretical treatment includes calculations of the rates of numerous excitation and decay processes based on nonlocal electron kinetics, and analysis of the transport equations for the resonance and metastable atoms. The solution technique of the Biberman-Holstein equation of radiation transport is developed in conformity with magnetron discharge geometry. The radial profile of the effective lifetime is obtained, taking into account radiation escape on the inner and outer electrodes. The distinction in formations of the radial profiles of the resonance and metastable atoms caused by specifics of radiation transport and diffusion is demonstrated. The results of experiments and calculations are compared.

I. INTRODUCTION

Magnetron discharges of various designs are widely employed in plasma enhanced deposition technologies to reach high sputtering rates. A quantitative study of the plasma becomes simpler in a cylindrical magnetron discharge (CMD) where inhomogeneities of the plasma parameters occur in a radial direction only and where the magnetic field is generated by coils and not by permanent magnets.

The absorption spectroscopy with diode lasers, which is an easy and versatile method of measuring particle densities, was used to determine the population densities in three of the four first excited levels of argon $^1P_1$, $^3P_1$, and $^3P_2$ or in Paschen notation $1s_2$, $1s_4$, and $1s_5$. Especially, the metastable levels cannot be accessed by other methods. Of special interest is the metastable level $1s_5$ due to the fact that the electron energy decreases in the positive column and the carrier production is supported by stepwise ionization of excited, long-lived levels.

Modeling of spatial distributions of the metastable and resonance atoms in the discharge of the magnetron configuration requires, in addition to an accurate calculation of the excitation rates, analysis of the transport processes connected with the diffusion of the metastable atoms and resonance radiation imprisonment in magnetron discharges. The recently developed nonlocal kinetic model of magnetron discharge plasmas [1] permits one to solve the spatially inhomogeneous Boltzmann kinetic equation in crossed electric and magnetic fields, and also allows one to calculate the electron distribution function and to compute the macroscopic properties, such as electron density and average energy, rates of excitation and ionization, etc. The solution of the problem on the metastable atom diffusion reveals no particular difficulties and can be obtained by standard methods. Formation of the resonance atom densities described by the Biberman-Holstein equation [2,3] requires special attention to geometrical properties of the discharge gap. Cylindrical magnetron discharge is represented by two extended coaxial electrodes in the axially homogeneous magnetic field generated by coils. The photons of resonance radiation can escape from the discharge not only on the outer bounding surface, as happens in cylindrical discharge tubes, but also on the inner one.

The issues on the population of resonance states in cylindrical discharge tubes are studied in some detail for Doppler and Lorentz profiles of spectral lines both under the assumption of the effective lifetime, and taking into account higher radial modes. There are numerous analytical and numerical methods [4–10] for solving the Biberman-Holstein equation in various geometrical situations; however, the discharge of magnetron configuration has not been considered in the literature. At the same time, the experimental data on populations of metastable and resonance atoms in magnetron discharge require development of an appropriate theoretical description.

In the present paper, we study experimentally and theoretically the formation of the spatial distributions of the excited atoms in magnetron discharge in argon at magnetic field strength $B=20$ mT, pressure $p=2.8$ Pa (gas temperature 300 K), and current 72 mA. The solution technique of the Biberman-Holstein equation is developed in conformity with magnetron discharge geometry. The approximation of the effective lifetime is considered and the radial dependence of the effective probability of radiation escape obtained for the discharge between two cylindrical electrodes. The balance equations for the particle densities of metastable and resonance atoms are considered, taking into account the excitation and decay processes that take place in the real discharge. The results of experiment and calculations are compared and discussed.

II. EXPERIMENTAL INVESTIGATIONS OF ELECTRON AND EXCITED ATOM DENSITIES

The experimental setup is shown in Fig. 1. The cylindrical magnetron discharge consists of a coaxial nonmagnetic stainless-steel vacuum vessel that can be pumped by the combination of a mechanical and turbomolecular pump down to pressures of the order of 10^{-3} Pa. The inner stainless-steel cylinder is water cooled, isolated from the
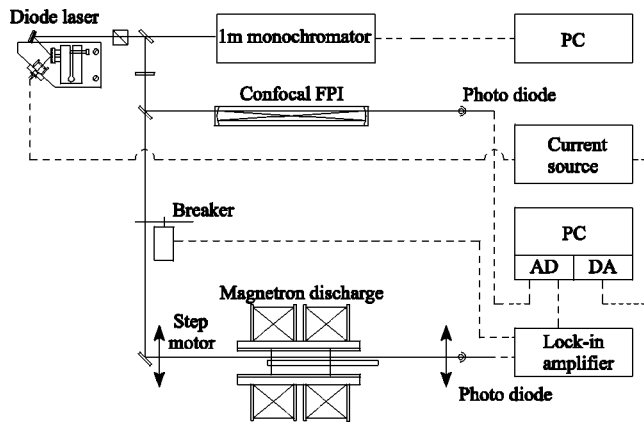
FIG. 1. Experimental setup for absorption measurements.

vacuum system body, and serves as cathode of the magnetron discharge that is connected to the negative output terminal of a high-voltage power supply with grounded positive output terminal. The outer cylinder serves as anode. The magnetic field is created by means of a pair of coils that were specially designed to have nearly parabolic cross sections in order to compensate for the losses at the ends of the coils and provide a homogeneous field strength distribution along the whole length of the discharge. The discharge current is stabilized by the power supply that is operated in a constant-current mode. The flow of the working gas to the discharge chamber has been controlled by using the MKS mass-flow controller, and the working pressure inside the discharge vessel has been measured by means of an MKS Baratron capacitance vacuummeter. The length of the discharge is adjusted by the two diaphragms kept at cathode potential. Four slots were cut in the diaphragms for the spectroscopic observations.

The laser setup consists of a holographic grating stabilized diode laser in the Littrow configuration with an obtained bandwidth of 4.5 MHz and a tuning range of approximately 25 GHz. The wavelength scanning was achieved by a computer controlled voltage ramp to a highly stabilized cur-

rent source that had less than 10 μA noise at typical operating currents of 100 mA. The whole laser setup was mounted on a heat sink that was actively temperature stabilized by a Peltier element to ± 2 mK. Passive temperature stabilization was achieved by a Perspex housing. Controlling of the laser frequency was done by a 1 m monochromator. Transmission peaks of a confocal Fabry-Perot resonator were used as frequency marks while scanning the laser across the absorption profile. By moving simultaneously the coupling mirror and the photodiode by means of a stepping motor unit the laser beam could be scanned across the diameter of the discharge in order to examine radial density and temperature profiles. The radial resolution due to the stepping motor is 1/48 mm. The signal is recorded using lock-in techniques in order to obtain low-noise measurements.

The tungsten cylindrical probe is positioned perpendicular to the discharge axis and hence also to electric and magnetic field lines. The probe is radially movable by a micrometer screw with an accuracy of ± 0.05 mm. The probe characteristic was measured by using a computer-controlled Siemens voltage calibrator B3050 and a Siemens multimeter B3220. The electron density was determined from the electron probe current I_{e0} at the plasma (space) potential V_s. Details on probe construction and measurements are contained in Refs. [11,12].

Spectroscopic measurements were done on the argon radiative transitions $(3p^5 4s-3p^5 4p)$ in the range 810–826 nm. A typical example for the absorption spectrum of the argon transition $1s_2-2p_2$ is shown in Fig. 2. To obtain the radial density and temperature profiles an efficient least squares routine [13] was used to fit the Gaussian absorption profiles for the different Zeeman transitions in a longitudinal magnetic field with known values of the magnetic field, Landé factors [14], and oscillator strengths [15]. Especially, for the Ar $1s_5$ level care has to be taken of the optical thickness that affected the absorption profile. The single Zeeman transitions were fitted with Doppler profiles. The temperature of the argon atoms defined from the Doppler linewidth is found to
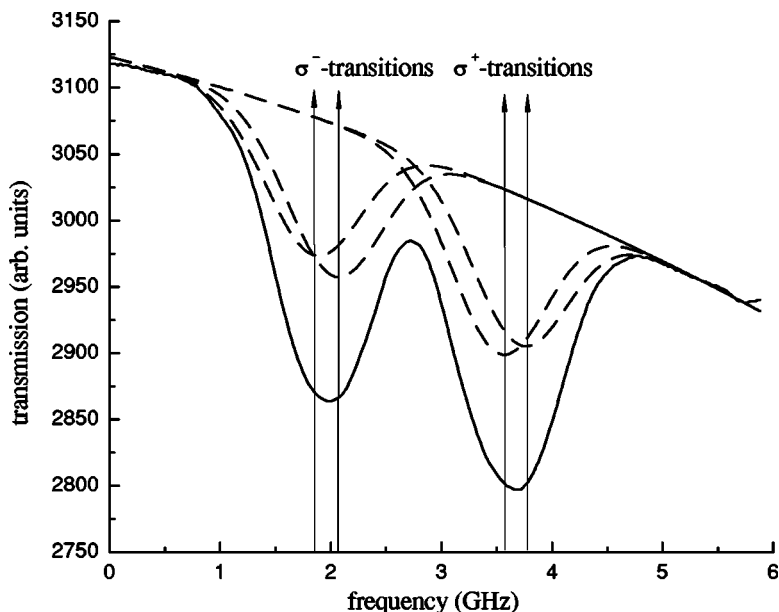

FIG. 2. Absorption spectrum of the argon transition $1s_2-2p_2$ measured at $p=1.5$ Pa, $B=485$ G, $i=100$ mA (solid line). The position of the single Zeeman components (dashed lines) is shown. The temperature of the argon atoms can be calculated from the Doppler width of the Gaussian profiles ($T=380\pm20$ K).

be almost constant along the discharge length and equal to 380 K.

III. TRANSPORT EQUATIONS AND EXCITATION RATES

The spatial distribution of the resonance atoms is described by the Biberman-Holstein integral equation

$$AN_r(\mathbf{r}) - A \int_{(V)} K(\mathbf{r},\mathbf{r}')N_r(\mathbf{r}')d^3r' = S(\mathbf{r}) - D(\mathbf{r}), \quad (1)$$

where S, D are, respectively, the rates of excitation and deexcitation of the resonance level, $N_r(\mathbf{r})$ is the resonance atom density at the point $\mathbf{r}$, A is the probability of spontaneous radiation, $K(\mathbf{r},\mathbf{r}')$ is the probability that a photon emitted at the point $\mathbf{r}'$ will travel the distance $|\mathbf{r}-\mathbf{r}'|$ without absorption and be absorbed at the point $\mathbf{r}$:

$$K(\mathbf{r},\mathbf{r}') = \frac{1}{4\pi} \frac{1}{(\mathbf{r}-\mathbf{r}')^2} \int_0^\infty \varepsilon_\nu k_\nu \exp(-k_\nu|\mathbf{r}-\mathbf{r}'|)d\nu. \quad (2)$$

Here ε_ν and k_ν are the profiles of emission and absorption lines.

The metastable atoms under the same approximations are described by the diffusion equation in the form

$$-D_m \frac{1}{r} \frac{d}{dr} r \frac{dN_m(r)}{dr} = S(r) - D(r), \quad (3)$$

where $S(r)$, $D(r)$, and $N_m(r)$ are the excitation and deexcitation rates and density of metastable atoms; D_m is the diffusion coefficient. Metastable and resonance atoms have to be treated differently, since the metastable atoms have a finite mean free path, while the photons in the wings of spectral lines travel very large distances and it is not possible to introduce a diffusion coefficient for these photons.

The self-consistent kinetic approach to the description of magnetron discharge developed in Ref. [1] permits one to solve the kinetic equation in spatially inhomogeneous electric fields, and also allows one to obtain the electron distribution function $f_0(U,r)$ as a function of the kinetic energy U and radial coordinate r and to compute macroscopic properties of the discharge, such as particle and current densities, excitation and ionization rates, etc.

In crossed electric (E) and magnetic (B) fields the kinetic equation for the electron distribution function takes the following representation:

$$\frac{U}{3} \frac{1}{r} \frac{\partial}{\partial r} r f_{1r}(U,r) - \frac{eE(r)}{3} \frac{\partial}{\partial U} U f_{1r}(U,r) = C_0(f_0), \quad (4)$$

$$f_{1r}(U,r) = \frac{\lambda_e}{1+(\lambda_e/r_{ec})^2} \left[-\frac{\partial f_0}{\partial r} + eE(r)\frac{\partial f_0}{\partial U} \right] \quad (5)$$

where the collision operator

$$C_0(f_0) = C_0^{el}(f_0) + C_0^{ex}(f_0) + C_0^{di}(f_0) + C_0^{si}(f_0)$$

includes elastic and inelastic collisions, direct and stepwise ionization collisions, respectively. λ_e is the electron free path and $r_{ec} = v/\omega_{eB}$ is the Larmor radius of electron cyclotron motion ($\omega_{eB} = eB/m$, v is the velocity of electron with the mass m and charge $-e$). By changing variables from U to the total energy $\varepsilon = U + e\varphi(r)$, with radial potential energy $e\varphi(r) = -\int_{R_a}^r E(r)dr(-e)$, the system (4), (5) can be simplified and the distribution function $f_0(U,r)$ calculated [1].

With the distribution function obtained, the rates of excitation and decay can be calculated for each level N_s of the system $3p^5 4s$, if the cross sections of the corresponding processes are known. These rates have to be substituted into the balance equations (1), (3) and the required densities of the excited states found.

The most important processes of excitation (S) and deexcitation (D) of the resonance and metastable states $4s$ in argon are the direct excitation by electron collision, cascade processes going through higher p levels with further radiation into s states, mixing of s states by electron collision, and chemoionization.

The right-hand sides of the balance equations (1) and (3) contain the following processes leading to population and quenching of excited states in real discharge.

(a) Excitation processes:

(i) Direct excitation by electron collision: $A+e \rightarrow A_m+e$. The rate of the process is

$$S_{0m}(r) = N\left(\frac{2}{m}\right)^{1/2} \int_{U_m}^\infty Q_{0m}(U)f_0(U,r)U dU.$$

(ii) Mixing in the system of s states by electron collision: $A_s+e \rightarrow A_m+e$,

$$S_{sm}(r) = \sum_{s\neq m} N_s\left(\frac{2}{m}\right)^{1/2} \int_{U_{sm}}^\infty Q_{sm}(U)f_0(U,r)U dU.$$

(iii) Cascade excitation of the atom from ground state into a p state by electron impact with further radiative transition to s state: $A+e \rightarrow A_p+e$, $A_p \rightarrow A_m+h\nu$,

$$S_{c0m}(r) = \sum_{p=1}^{10} \left(\frac{NA_{pm}}{\sum_k A_{pk}} \left(\frac{2}{m}\right)^{1/2} \int_{U_p}^\infty Q_{0p}(U)f_0(U,r)U dU \right).$$

(iv) Cascade excitation of the atom in s state into one of the p states with further radiative transition to s state: $A_s +e \rightarrow A_p+e$, $A_p \rightarrow A_m+h\nu$,

$$S_{csm}(r) = \sum_{s\neq m} N_s \left[\sum_{p=1}^{10} \left(\frac{A_{pm}}{\sum_k A_{pk}} \left(\frac{2}{m}\right)^{1/2} \right. \right.$$
$$\left. \left. \times \int_{U_{sp}}^\infty Q_{sp}(U)f_0(U,r)U dU \right) \right].$$

(b) Deexcitation processes:

(i) Mixing in the system of s states by electron collision: $A_m + e \rightarrow A_s + e$,

$$D_{ms}(r) = N_m \sum_{s \neq m} \left(\frac{2}{m} \right)^{1/2} \int_{U_{sm}}^{\infty} Q_{sm}(U) f_0(U,r) U dU.$$

(ii) Cascade mixing in the system of s states as a result of stepwise excitation of the atom from the s state into one of the p state with further radiative transition on the s level: $A_m + e \rightarrow A_p + e$, $A_p \rightarrow A_s + h\nu$,

$$D_{cms}(r) = N_m \sum_{p=1}^{10} \left(1 - \frac{A_{pm}}{\sum_k A_{pk}} \right) \left(\frac{2}{m} \right)^{1/2}$$

$$\times \int_{U_{mp}}^{\infty} Q_{mp}(U) f_0(U,r) U dU.$$

(iii) Stepwise ionization: $A_m + e \rightarrow A^+ + 2e$,

$$D_{m\infty}(r) = N_m \left(\frac{2}{m} \right)^{1/2} \int_{U_{m\infty}}^{\infty} Q_{m\infty}(U) f_0(U,r) U dU.$$

Here N is the gas density, N_k is the atom density in the kth state of the system $4s$, U_m is the excitation energy of the level m [14], $U_{sp} = U_p - U_s$ is the process threshold, $U_{sm} = U_m - U_s$ for collisions of the first kind and is zero for collisions of the second kind. Details about cross sections used in the calculations are given in the Appendix. The oscillator strengths of the radiative transitions $p \rightarrow s$ [15] are listed in the Appendix. The mixing processes by atom collisions were neglected due to their smallness at low pressures.

The formation of the excited state densities was beyond the scope of the prevous paper [1], where the main attention was given to a self-consistent description of the electron and ion components and field formation. The metastable atoms were treated there approximately under the assumption of the effective excited level with the given density distribution. In this study, we concentrate mainly on the transport processes governing the formation of each resonance and metastable level.

IV. ANALYSIS OF RADIATION TRANSPORT EQUATION FOR MAGNETRON DISCHARGE

In this section, the integral equation for radiation transport will be considered with respect to magnetron discharge geometry. In order to elucidate the transport and imprisment features of radiation, the analysis of the Biberman-Holstein integral equation will be given while neglecting the mixing processes, which is in the form

$$W_r(\mathbf{r}) = AN_r(\mathbf{r}) - A \int_{(V)} K(\mathbf{r},\mathbf{r}') N_r(\mathbf{r}') d^3 r', \qquad (6)$$

where $W_r(\mathbf{r})$ is the source term, independent of the density N_r.
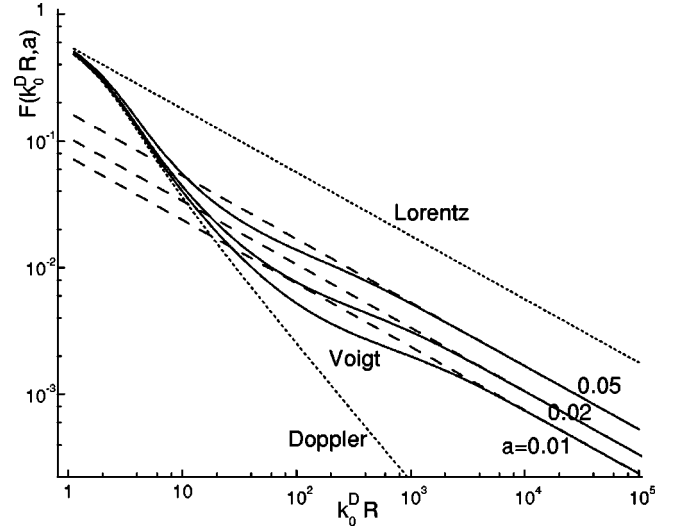

FIG. 3. Dependence of the function $F(k_0^D R, a)$ on the absorption coefficient at the center of the Doppler part of the Voigt profile k_0^D for different parameters of the Voigt profile a. Dotted lines correspond to calculations with pure Lorentzian and Doppler line profiles. Dashed lines are the calculations by asymptotical formula (9).

A. Influence of the line profile

In a range of magnetron discharge working pressures the profiles of spectral lines are described by the Voigt function with a small value of the parameter $a = (\ln 2)^{1/2} \Delta \nu_L / \Delta \nu_D$:

$$\varepsilon_\omega(a,\omega) = \frac{a}{\pi^{3/2}} \int_{-\infty}^{\infty} \frac{\exp(-y^2) dy}{(\omega - y)^2 + a^2}, \qquad (7)$$

$$k_\omega = k_0^D \pi^{1/2} \varepsilon_\omega; \qquad \omega = 2(\ln 2)^{1/2} (\nu - \nu_0)/\Delta \nu_D.$$

$\Delta \nu_L$ and $\Delta \nu_D = 2(\ln 2)^{1/2} (2kT/M)^{1/2} \nu_0/c$ are the half-widths of Lorentzian and Doppler profiles. The half-width of the Lorentzian profile is stipulated by natural broadening with $\Delta \nu_L^n = A/2\pi$ and the collisional one $\Delta \nu_L^c = (g_0/g_r)^{1/2} e^2 N f/(11.7 \pi^2 m \nu_0 \epsilon_0)$. ν_0 is the frequency of the resonance transition, $k_0^D = AN(c^2/\nu_0^2)(g_r/g_0)(\ln 2)^{1/2}/(4\pi^{3/2} \Delta \nu_D)$ is the absorption coefficient at the center of the Doppler line, g_r and g_0 are the statistical weights of the resonance and ground states, f is the oscillator strength, c is the light velocity, and ϵ_0 is the vacuum permittivity.

A very important property in the theory of radiation transport is the function

$$F(k_0^D R, a) = \int_{-\infty}^{\infty} \varepsilon_\omega \exp(-k_\omega R) d\omega, \qquad (8)$$

which strongly depends on the profile of the spectral line. The dependence of the calculated values of this function on the optical thickness $k_0^D R$ (R is the tube radius) is shown in Fig. 3 for several values of the Voigt profile parameter (solid lines). In the same figure the asymptotics of these functions calculated with the Doppler profile and Lorentzian wing of the Voigt profile are shown,
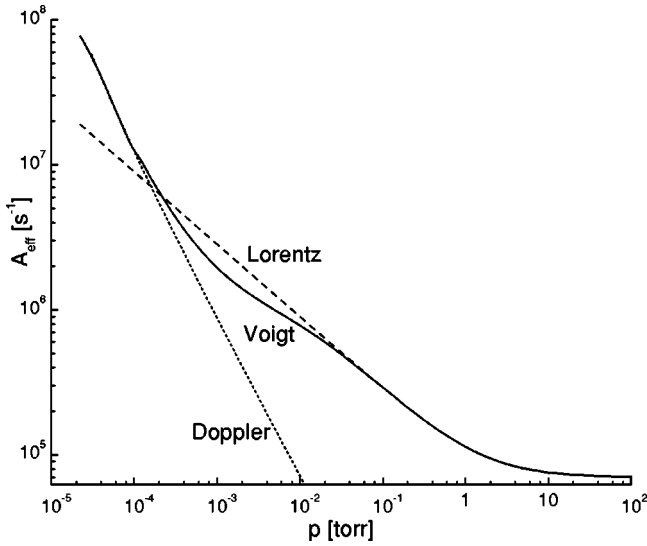
FIG. 4. Effective probability of radiation escape from an infinite cylindrical tube of radius 3 cm dependent on gas pressure. Solid line corresponds to the Voigt profile and dashed lines to the Lorentzian and Doppler line profiles. Ar, transition $^1P_1 - ^1S_0$.

$$F(k_0^D R, a) \approx \frac{1}{k_0^D R [\pi \ln(k_0^D R)]^{1/2}} \quad \text{(Doppler),}$$

$$F(k_0^D R, a) \approx \pi^{1/4} \left(\frac{a}{\pi k_0^D R} \right)^{1/2} \quad \text{(Lorentz).} \quad (9)$$

It is seen from the figure that even for the minimal value of $a=0.01$, the Lorentz asymptotic is applicable beginning with the optical thickness $k_0^D R \sim 3 \times 10^3$. With the growth of the parameter a the applicability range of the asymptotical solution increases towards smaller optical densities. Thus, at $k_0^D R > 3 \times 10^3$ that is observed in experiments, the central part of the Voigt profile is absorbed, and when calculating the kernel of Eq. (1) the Voigt profile can be replaced with the Lorentzian one written in the form

$$k_\omega = \frac{a}{\pi^{1/2}} \frac{k_0^D}{a^2 + \omega^2}, \qquad \varepsilon_\omega = \frac{a}{\pi} \frac{1}{a^2 + \omega^2}.$$

With the help of the function (8) the effective probability A_{eff} of radiation escape from the axis of an infinite cylindrical tube can be easily calculated by Biberman's theory [4], dependent on gas pressure. With increasing pressure and number of absorbing atoms the optical thickness grows, and collision broadening leads to an increase of the parameter a of the Voigt profile.

In Fig. 4, the effective probability of a photon escape from the axis of a tube is given for the argon transition $^1P_1 - ^1S_0$ ($A = 4.3 \times 10^8$ s^{-1}, $\nu_0 = 2.86 \times 10^{15}$ s^{-1}, $f = 0.213$). It is seen from the figure that the Doppler asymptotic, which gives $A_{eff} = 0.785A/(k_0^D R [\pi \ln(k_0^D R)]^{1/2})$, can be used at pressures below about 10^{-4} Torr. At pressures above about 2×10^{-2} Torr the Lorentzian asymptotic is applicable with A_{eff}

$= 0.874A(\pi k_0^L R)^{-1/2}$. For the pressures exceeding 1 Torr the effective probability becomes independent of pressure, since the absorption coefficient under these conditions is determined by collision broadening.

The presence of a magnetic field of the order of hundreds of Gauss and Zeeman splitting of the order of natural width caused by this field, does not play any role in calculations since under large absorption coefficients the central part of the profile is completely absorbed.

In the following we shall consider magnetron discharge at low pressures ($p < 0.05$ Torr) where pressure broadening occurs to be smaller than the natural one and the parameter a becomes equal to 0.017 for the above transition. The absorption coefficient at the center of the line has large values $k_0^D [\text{cm}^{-1}] = 1.58 \times 10^{-12} N [\text{cm}^{-3}]$ that lead to complete absorption of the Doppler part of the profile at short distances and permits us to employ the Lorentzian asymptotic of the Voigt profile.

B. Approximation of the effective lifetime for magnetron discharge

The radial dependence of the effective lifetime τ_{eff} or the effective probability of radiation escape A_{eff} by Biberman's theory [4] can be obtained if one eliminates the density $N(\mathbf{r}')$ at the point $\mathbf{r}$. This can be done if the kernel $K(|\mathbf{r} - \mathbf{r}'|)$ decreases more abruptly than the density $N_r(\mathbf{r}')$,

$$A_{eff}(\mathbf{r}) = A \left[1 - \int_{(V)} K(|\mathbf{r} - \mathbf{r}'|) d^3 r' \right]. \quad (10)$$

Integration over the discharge volume in Eq. (10) includes integration over the magnetron length [Fig. 5(a)] and the area unscreened by the inner electrode shown in Fig. 5(b). Defining by z the axial distance between the points $\mathbf{r}$ and $\mathbf{r}'$, and by ρ the distance between these points in the plain $z = $ const, we may write $|\mathbf{r} - \mathbf{r}'|^2 = z^2 + \rho^2$, $r'^2 = r^2 + \rho^2 - 2r\rho \cos \psi$. The integral in Eq. (10) becomes

$$\int_{(V)} K(\mathbf{r}, \mathbf{r}') d^3 r' = \int_0^{\psi_0} d\psi \int_0^{\rho_C} \rho d\rho H(\rho, \psi)$$
$$+ \int_{\psi_0}^{\pi} d\psi \int_0^{\rho_A} \rho d\rho H(\rho, \psi),$$

where $\psi_0 = \arcsin(R_C / r)$,

$$H = \frac{1}{2\pi} \int_{-\infty}^{\infty} \frac{dz}{z^2 + \rho^2} \int_0^{\infty} k_\nu \varepsilon_\nu \exp[-k_\nu (z^2 + \rho^2)^{1/2}] d\nu,$$

and the limits of integration over ρ are defined by expressions

$$\rho_C = r \cos \psi - (R_C^2 - r^2 \sin^2 \psi), \quad \psi_0 < \psi < \pi,$$

$$\rho_A = r \cos \psi + (R_A^2 - r^2 \sin^2 \psi), \quad 0 < \psi < \psi_0,$$

where R_C and R_A are the radii of inner cathode and outer anode.
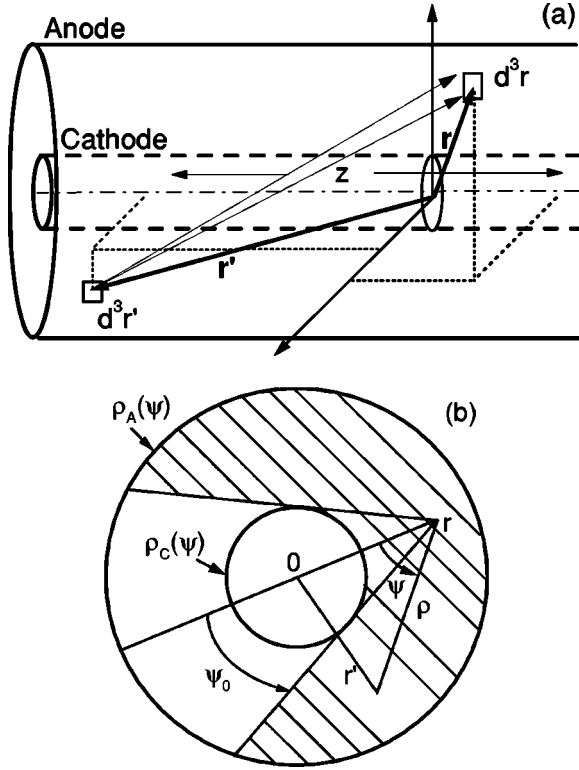
FIG. 5. Scheme of magnetron discharge and resonance radiation propagation (a). Magnetron cross section at $z=$const (b). The integration over the volume in Eq. (10) is equivalent to integration over the dashed region and along the discharge length.

By introducing the variable $x=z/\rho$ instead of z, we obtain

$$
\int_{(V)} K(\mathbf{r},\mathbf{r}')d^3r'
$$

$$
= \frac{1}{\pi}\int_0^{\psi_0} d\psi \int_0^\infty \frac{dy}{(y^2+1)^{3/2}}
$$

$$
\times \int_0^\infty \varepsilon_\nu\{1-\exp[-k_\nu\rho_C(y^2+1)^{1/2}]\}d\nu
$$

$$
+ \frac{1}{\pi}\int_{\psi_0}^{\pi} d\psi \int_0^\infty \frac{dy}{(y^2+1)^{3/2}}
$$

$$
\times \int_0^\infty \varepsilon_\nu\{1-\exp[-k_\nu\rho_A(y^2+1)^{1/2}]\}d\nu.
$$

$$(11)$$

When taking the integral over frequency in Eq. (11) one should keep in mind that $\int_0^\infty \varepsilon_\nu d\nu=1$, and the integral $\int_0^\infty \varepsilon_\nu \exp(-k_\nu R)d\nu$ may be calculated by the asymptotical formula (9). Finally, for the Lorentzian asymptotic of the Voigt profile at large absorption densities we obtain

$$
A_{eff}(r)=A\frac{0.874}{(\pi k_0 R_A)^{1/2}}\frac{1}{\pi}\left[\int_0^{\psi_0}\frac{d\psi}{(q_C)^{1/2}}+\int_{\psi_0}^{\pi}\frac{d\psi}{(q_A)^{1/2}}\right],
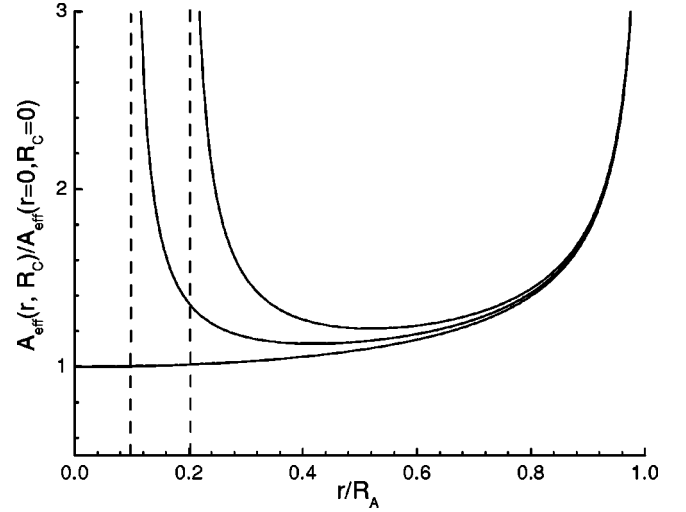$$

$$(12)$$

FIG. 6. Effective lifetime as a function of radial position and radius of cathode. The ratio R_C/R_A equals 0, which corresponds to the cylindrical discharge tube; 0.1;0.2.

where $q_{C,A}=\rho_{C,A}/R_A$ and the absorption coefficient at the center of line is $k_0=k_0^D/(a\pi^{1/2})=k_0^L$, with $k_0^L=AN(c^2/\nu_0^2)(g_r/g_0)/(4\pi^2\Delta\nu_L)$ denoting the absorption coefficient at the center of the Lorentzian line. The radial dependencies of A_{eff} calculated according to Eq. (12) are represented in Fig. 6 for various ratios of electrode radii R_C/R_A. It is seen from the figure that the effective probability of radiation escape increases in the vicinity of both electrodes. For comparison, the radial dependence of A_{eff} for a cylindrical tube without a central electrode ($R_C\to0$) is shown in the same figure.

The calculations with the Doppler profile result in

$$
A_{eff}(r)=\frac{A}{\pi}\frac{0.785}{k_0^D R_A[\pi\ln(k_0^D R_A)]^{1/2}}\left[\int_0^{\psi_0}\frac{d\psi}{q_C}+\int_{\psi_0}^{\pi}\frac{d\psi}{q_A}\right].
$$

This case is realized at very low pressures ($p<10^{-3}$ Torr), but at high absorption densities $k_0^D R>10$.

C. Eigenmodes and eigenvalues of the transport equation

To find eigenvalues and eigenmodes of the transport equation (6) various methods may be applied. One of the simplest ways consists in replacement of the integral equation (6) by a system of linear algebraic equations. By dividing the interelectrode distance into M intervals and assuming the density of the resonance atoms within each interval to be constant, the integral term in Eq. (6) can be written in the form

$$
\int_{(V)} K(\mathbf{r},\mathbf{r}')N_r(\mathbf{r}')d^3r'
$$

$$
= \sum_{m=0}^{M-1} N_r(r_{m+1/2})\int_{r_m}^{r_{m+1}} K(r,r')r'\,dr'\,dz\,d\psi.
$$

Integration of the kernel within the limits $r_m<r'<r_{m+1}$ gives a matrix of the coefficients $b_{k,m}$. The resulting system of linear equations to define the densities $N_r(r_k)$ has the form

$$A \frac{0.874}{(\pi k_0^L R)^{1/2}} \left[\sum_{m=0}^{M-1} N_r(r_{m+1/2}) b_{k,m} \right] = W(r_{k+1/2}). \quad (13)$$

The coefficients of the matrix may be computed analogously to calculations of effective lifetime by the Lorentzian profile of absorption and emission. The following three cases should be distinguished here:

$r_k < r_m$,

$$b_{km} = \int_{\psi_0}^{\pi} d\psi \int_{\rho_m^+}^{\rho_{m+1}^+} \rho d\rho H(\rho, \psi)$$

$$= \frac{1}{\pi} \left[\int_{\psi_0}^{\pi} \frac{d\psi}{(q_m^+)^{1/2}} - \int_{\psi_0}^{\pi} \frac{d\psi}{(q_{m+1}^+)^{1/2}} \right];$$

$r_m < r_k < r_{m+1}$,

$$b_{km} = \int_{\psi_0}^{\pi} d\psi \int_{0}^{\rho_{m+1}^+} H \rho d\rho - \int_{\psi_0}^{\psi_m} d\psi \int_{\rho_m^-}^{\rho_m^+} H \rho d\rho$$

$$+ \int_{0}^{\psi_0} d\psi \int_{0}^{\rho_m^-} H \rho d\rho$$

$$= \frac{1}{\pi} \left[\int_{\psi_0}^{\psi_{m+1}} \frac{d\psi}{(q_m^+)^{1/2}} - \int_{\psi_0}^{\pi} \frac{d\psi}{(q_{m+1}^+)^{1/2}} \right.$$

$$\left. - \int_{0}^{\psi_m} \frac{d\psi}{(q_m^-)^{1/2}} \right];$$

$r_k > r_{m+1}$,

$$b_{km} = \int_{0}^{\psi_{m+1}} d\psi \int_{\rho_{m+1}^-}^{\rho_{m+1}^+} H \rho d\rho - \int_{0}^{\psi_m} d\psi \int_{\rho_m^-}^{\rho_m^+} H \rho d\rho$$

$$- \int_{0}^{\psi_0} d\psi \int_{\rho_m^+}^{\rho_{m+1}^+} H \rho d\rho = \frac{1}{\pi} \left[\int_{0}^{\psi_{m+1}} \frac{d\psi}{(q_{m+1}^-)^{1/2}} \right.$$

$$\left. - \int_{0}^{\psi_{m+1}} \frac{d\psi}{(q_{m+1}^+)^{1/2}} - \int_{0}^{\psi_m} \frac{d\psi}{(q_m^-)^{1/2}} + \int_{\psi_0}^{\psi_m} \frac{d\psi}{(q_m^+)^{1/2}} \right],$$

where the integration limits are defined as

$$\rho_m^- = r_k \cos \psi - (r_m^2 - r_k^2 \sin^2 \psi)^{1/2},$$

$$\rho_m^+ = r_k \cos \psi + (r_m^2 - r_k^2 \sin^2 \psi)^{1/2},$$

$$\psi_m = \arcsin(r_k / r_m),$$

$$\psi_0 = \arcsin(R_C / r_m).$$

The variable q differs from ρ by normalization on the anode radius: $q = \rho / R_A$.

In Fig. 7, the eigenmodes $\varphi(\tilde{r})$, where $\tilde{r} = r / R_A$ of the matrix $b_{k,m}$, are shown. The eigenfunctions are normalized according to the condition $\int_0^1 \varphi_i(\tilde{r}) \varphi_j(\tilde{r}) \tilde{r} d\tilde{r} = \delta_{ij}$ following from the symmetry of the integral equation kernel. The radial course of the fundamental mode is shown in Fig. 7(a) for
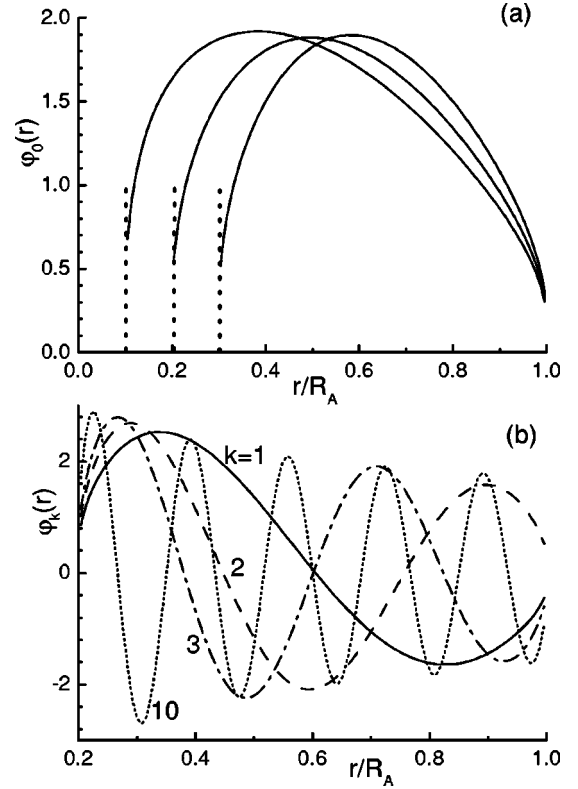

FIG. 7. Radial course of the fundamental modes of the kernel of the integral equation for different ratios R_C / R_A (a). Radial course of higher modes in magnetron configuration with $R_C / R_A = 0.2$ (b).

several ratios of electrode radii. In contrast to cylindrical tube geometry where the fundamental mode monotonically decreases from the axis towards the wall, in magnetron discharge this mode has a maximum. The radial dependencies of higher modes are illustrated in Fig. 7(b) for the ratio $R_C / R_A = 0.2$.

The results of a model problem on resonance atom distribution formation are shown in Figs. 8 and 9. The densities of a resonance state obtained from the accurate solution of the Biberman-Holstein equation, i.e., from system (13) (N_r, solid line) and in approximation of the effective lifetime (N_τ, dashed line) are shown in Fig. 8 for two profiles of the excitation rate (W, dotted line). The solutions are normalized by the conditions that the maximal value of $W_0 = 1$ and $W_0 / N_0 = A\lambda 0.874/(\pi k_0^L R_A)^{1/2}$, where $\lambda = 1.47$ is the eigenvalue of the fundamental mode for the particular magnetron configuration. It should be noted that in the case of a strong deviation of the excitation rate from the fundamental mode the densities calculated under approximation of effective lifetime differ noticeably (more than two times) from those calculated accurately.

In Fig. 9, the normalized radial profiles of the excitation rate and densities of resonance and metastable states are shown to demonstrate particularly the influence of diffusion of metastable atoms and the transport of resonance radiation for magnetron discharge geometry while neglecting the mixing processes. It is seen that diffusion of the metastables leads to significant broadening of the density profile in comparison to that of the source. The profile of the resonance
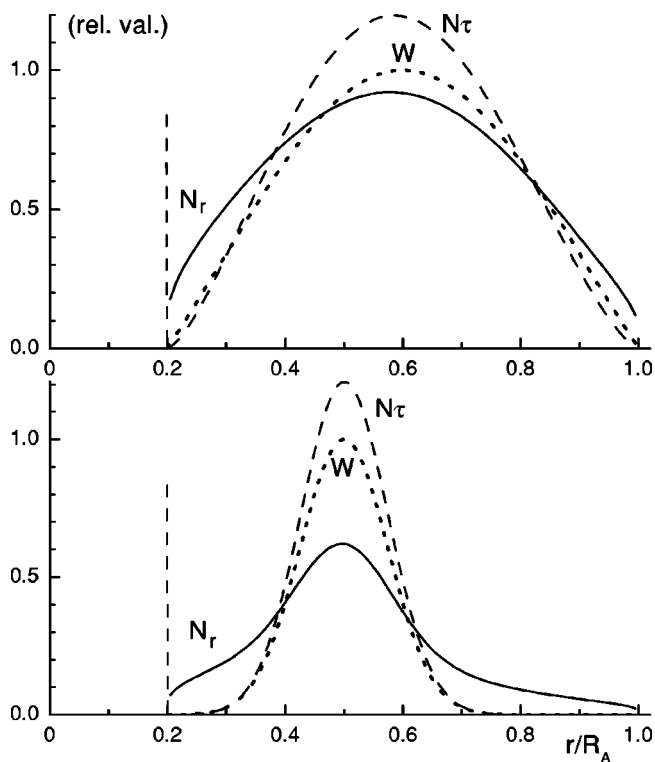
FIG. 8. Model radial distributions of excitation rate W and the densities of resonance atoms calculated under the assumption of effective lifetime N_τ and from the accurate solution of radiation transport equation (13) N_r for broad (a) and narrow (b) profiles of the source.

atom density is similar to the profile of the source with the exception of the peripheral regions. If the mixing processes are important, the profiles of metastable and resonance atoms become more alike.

V. DISCUSSION OF THE RESULTS AND COMPARISON WITH EXPERIMENT

In this study the radial profile of the electric field strength was chosen in such a way that the electron distribution function calculated in this field gives the absolute values and
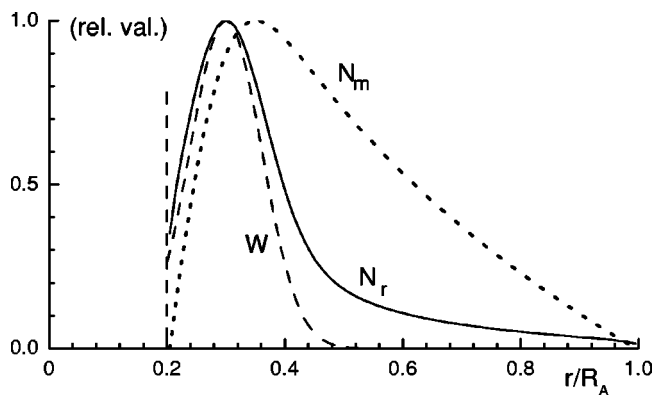

FIG. 9. Normalized radial distributions of the excitation rate W, metastable N_m, and resonance N_r atom densities formed in magnetron discharge while neglecting the mixing processes.
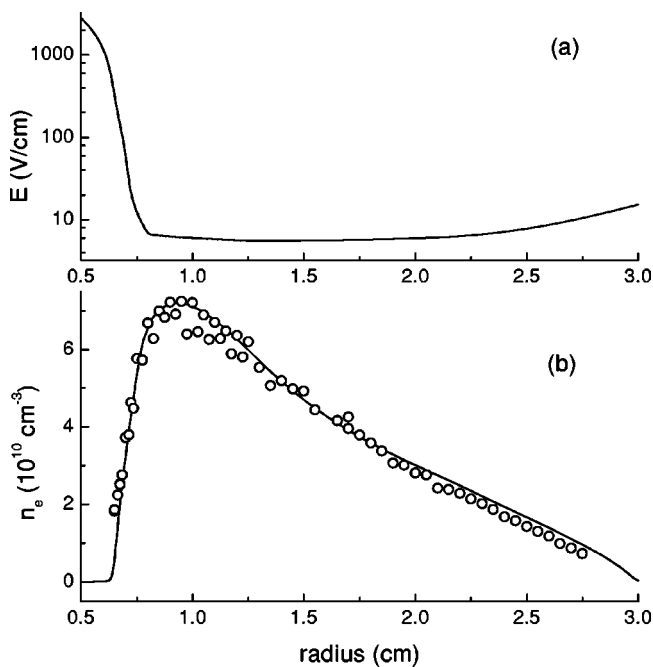

FIG. 10. Model electric field strength as a function of radial position in magnetron discharge (a). The electron distribution function calculated in this field gives the electron density (line) coincident with the measured (dots) profile (b).

radial profile of the electron density equal to the experimentally measured density of electrons. The radial dependence of the electric field strength is shown in Fig. 10(a). The electron density that corresponds to the electron distribution function that is formed in this field has a radial dependence as shown in Fig. 10(b). The electric field profile shown in Fig. 10(a) is in a good correlation with the field profile obtained self-consistently in Ref. [1]. With the help of the distribution function the rates of excitation and decay were calculated as functions of radial position.
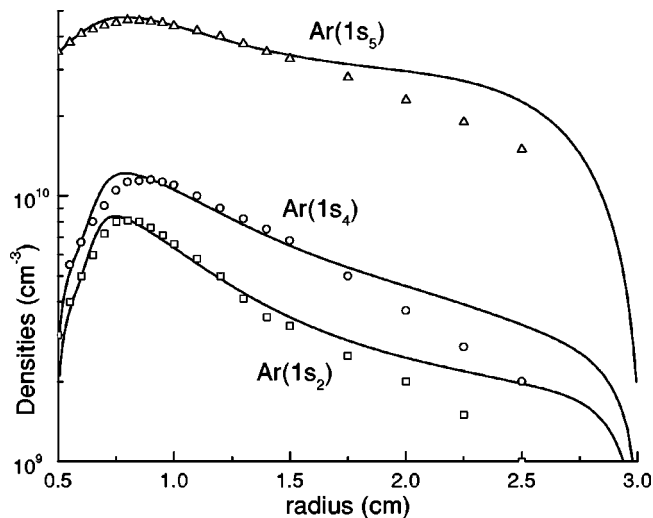

FIG. 11. Densities of the excited Ar states in real magnetron discharge. Symbols are the data of experiment. Solid lines are the results of calculations.

TABLE I. Oscillator strengths for the transitions $p \rightarrow s$.

	s_2	s_3	s_4	s_5
p_1	0.1330	0	0.00054	0
p_2	0.1720	0.341	0.0159	0.0292
p_3	0.4310	0	0.1190	0.0296
p_4	0.1600	0.560	0.0002	0.00299
p_5	0	0	0.1210	0
p_6	0.1250	0	0	0.239
p_7	0.0151	0.095	0.2730	0.0306
p_8	0.0385	0	0.4130	0.092
p_9	0	0	0	0.51
p_{10}	0.0049	0.058	0.0840	0.159

TABLE II. Coefficients C_p used in calculations.

p	1	2	3	4	5	6	7	8	9	10
C_p	5	15	6	15	8	14	16	15	6	10

Equations (1) and (3) were transformed into the system of linear algebraic equations in a way analogous to that described in the previous section. Finally, to determine the excited atom densities, we obtained the following system of linear equations:

$$\hat{M}\vec{N}_s = \vec{W}_s. \qquad (14)$$

The vector $\vec{N}_s$ has the components N_2, N_3, N_4, N_5 that are the densities of the resonance and metastable atoms.

The components of the free term, i.e., of the vector $\vec{W}_s$ correspond to direct and cascade excitation of the level N_s. Diagonal elements of the matrix $\hat{M}$ represent the decay frequencies of the level N_s by stepwise ionization, diffusion, and radiation decay; direct mixing in s levels by electron collisions; and cascade collision-radiative mixing through higher p levels. Nondiagonal elements of the matrix are connected with the population processes of the level N_s by stepwise and cascade collision-radiative mixing.

The solution of the system of $4 \times M$ equations (14) permits us to find the radial dependencies of the densities $\mathrm{Ar}(1s_{2-5})$.

In Fig. 11, the calculation results of the particle number densities of the s_2, s_4, and s_5 levels are compared with the data obtained in experiments for the following discharge conditions: Ar, $B = 20$ mT, $p = 2.8$ Pa, $i = 72$ mA, $R_C = 0.5$ cm, $R_A = 3$ cm, and discharge length $L = 12$ cm. The density profiles have a maximum at the boundary of the cathode region and a positive column where the excitation rate attains maximal value, and then smoothly decrease towards the anode. Under our conditions the configuration $3p^5 4s$ of the argon atoms is populated mainly by the cascade processes going through direct excitation of $3p^5 4p$ states and subsequent radiation. The direct and, in particular, the cascade mixing processes are quite efficient, causing the decrease in the metastable and resonance densities to be similar.

The distribution of the metastable atoms is described quite well. In order to fit the experimental curve for the density of s_2 state, the probability of its spontaneous radiation was taken to be 2.5 times smaller than that given in the literature. We should note that the relative course of the density of the s_2 state is described well by the theory, but the absolute value, which depends on many factors shows the indicated deviation from the experimental data. This difference can be explained by the finite length of magnetron discharge, uncertainty in the constants of elementary processes, and strong sensitivity of the source term to the value of the electric field. As soon as the excitation cross section and the probability of resonance radiation have the largest values for the state s_2, these reasons can result in the largest error, namely, for the density $\mathrm{Ar}(1s_2)$.

VI. CONCLUSION

In the present paper, the densities of argon atoms in the resonance and metastable $3p^5 4s$ states were measured by the laser absorption technique. The excitation rates of these states by direct electron collision and cascade transitions over radiating p levels are calculated on the basis of the nonlocal electron distribution function. The Biberman-Holstein resonance radiation transport equation is analyzed in conformity with cylindrical magnetron geometry. The kernel of the integral operator is considered in the explicit form. The effective probabilities of radiation escape are calculated dependent on the radial coordinate for various values of cathode and anode radii. The solution of the integral radiation transport equation is obtained by its transformation into the system of linear equations. Eigenmodes and eigenvalues are found that permit one to consider the influence of higher modes on the formation of spatiotemporal distributions of the resonance atoms. The distinctions in radial profiles of the resonance and metastable atoms are demonstrated, which are caused by peculiarities of the processes of radiation transport and diffusion. The results of the calculations are compared to those of experimental study.

ACKNOWLEDGMENTS

APPENDIX

The cross sections Q_{0m} and Q_{0p} of direct excitation of the s and p levels were taken according to data [16].

When calculating the rates S_{sm} and D_{ms}, one needs to distinguish the collisions of the first and second kinds. The corresponding cross sections were taken from Ref. [17] in the form

$$Q_{sm}(U) = 4\pi a_0^2 f_{sm} \frac{\mathrm{Ry}^2}{U_{sm}} \left[\frac{U - U_{sm}}{U^2} \right] \quad \text{(first kind)},$$

$$Q_{sm}(U) = 4\pi a_0^2 f_{sm} \frac{g_m}{g_s} \frac{Ry^2}{U_{sm}} \left[\frac{1}{U}\right] \quad \text{(second kind)},$$

where a_0 is the radius of the first Bohr orbit, Ry is the Rydberg coefficient, $U_{sm} = |U_m - U_s|$ is the difference of excitation energies, g_s is the statistical weight of the level s, f_{sm} are the oscillator strengths that were taken as the following: $f_{35} = f_{53} = 0.0084$, $f_{45} = f_{54} = 0.0085$, $f_{52} = f_{25} = 0.007$. The values for other transitions $s \rightarrow s$ were taken equal to 0.001.

The cross section Q_{sp} for stepwise excitation $s \rightarrow p$ was calculated using the formula [18]

$$Q_{sp}(U) = 4\pi a_0^2 f_{ps} \frac{Ry^2}{U_{sp}^2} \left[\frac{x-1}{x}\right]^{1/2}$$

$$\times \frac{\ln\{2[x + (x^2 + x)^{1/2} - 1/2]\}}{x + C_p},$$

where $x = U/U_{sp}$, oscillator strengths are represented in Table I, and coefficients C_p, are listed in Table II.

[1] I.A. Porokhova, Yu.B. Golubovskii, J. Bretagne, M. Tichy, and J.F. Behnke, Phys. Rev. E **63**, 056408 (2001).

[2] T. Holstein, Phys. Rev. **72**, 1212 (1947); **83**, 1159 (1951).

[3] L.M. Biberman, Zh. Eksp. Teor. Fiz. **17**, 416 (1947).

[4] L. M. Biberman, V. S. Vorobjev, and I. T. Yakubov, *Kinetics of Nonequilibrium Low-Temperature Plasma* (Plenum, New York, 1987).

[5] A. G. Mitchell and M. W. Zeemanski, *Resonance Radiation and Excited Atoms* (Cambridge University Press, Cambridge, 1961).

[6] C. van Trigt, Phys. Rev. **181**, 97 (1969); Phys. Rev. A **13**, 726 (1976).

[7] A. F. Molisch and B. P. Oehry, *Radiation Trapping in Atomic Vapours* (Oxford University Press, Oxford, 1998).

[8] V. V. Ivanov, *Transfer of Radiation Ion Spectral Lines* (U.S. GPO, Washington, D.C., 1973).

[9] Yu.B. Golubovskii and R.I. Ljagushchenko, Opt. Spektrosk. **38**, 1086 (1975); **40**, 215 (1976).

[10] N.N. Bezuglov, A.F. Molisch, A.N. Klucharev, F. Fuso, and M. Allegrini, Phys. Rev. A **57**, 2612 (1998); **59**, 4340 (1999).

[11] P. Kudrna and E. Passoth, Contrib. Plasma Phys. **37**, 417 (1997).

[12] E. Passoth, P. Kudrna, C. Csambal, J.F. Behnke, M. Tichý, and V. Helbig, J. Phys. D **30**, 1763 (1996).

[13] K. Jess, V. Helbig, F. Greiner, J. Kaspareit, V. Rohde, and T. Weirauch, J. Quant. Spectrosc. Radiat. Transf. **41**, 69 (1989).

[14] C. E. Moore, *1949 Atomic Energy Levels* (National Bureau of Standards, Washington, D.C., 1949).

[15] W.L. Wiese, J.W. Brault, K. Danzmann, V. Helbig, and M. Kock, Phys. Rev. A **39**, 2461 (1989).

[16] M. Hayashi (private communication).

[17] J. Delcroix, C. M. Ferreira, and A. Ricard, *Principles of Laser Plasmas*, edited by G. Bekefi (Wiley, New York, 1976).

[18] J.F. Behnke, H. Deutsch, and H. Scheibner, Beitr. Plasmaphys. **25**, 41 (1985).